Supplementary Information

Dynamic single-molecule counting for the quantification and optimization of nanoparticle functionalization protocols

Matěj Horáček,[a,b] Dion J. Engels,[a] and Peter Zijlstra[*a,b]

[a] Faculty of Applied Physics, Eindhoven University of Technology, 5600 MB, Eindhoven, The Netherlands.
[b] Institute for Complex Molecular Systems, Eindhoven University of Technology, 5600 MB, Eindhoven, The Netherlands.
* m.horacek@tue.nl
† Corresponding author: p.zijlstra@tue.nl

Contents

S1 Sample preparation

We used single crystalline gold nanorods stabilized in cetyltrimethylammonium bromide (CTAB) purchased from *Nanoseedz*. First, the CTAB concentration in the suspension of nanorods was lowered to 1 mM, and the concentration of the particles was adjusted to yield a coverage of 500 - 600 particles in the 130 x 130 μm^2 field-of-view of the microscope after spin-coating.

A 50 µL drop of the suspension was then spincoated on a coverslip at 2000 rpm for 90 seconds. To ensure that the particles are firmly attached to the substrate, the coverslips were first functionalized with (3-Mercaptopropyl)trimethoxysilane (MPTMS). For thiolation we used the following protocol:

1. Clean coverslips by sonication in methanol for 20 mins.
2. UV/ozone clean coverslips for 90 mins.
3. Immerse coverslips in 5% v/v solution of MPTS in methanol for 3 minutes.
4. Rinse coverslips with methanol, then clean by sonication in methanol for 20 mins.

After the last wash in methanol the nanorods were immediately spincoated onto the coverslips. After spincoating the coverslips were rinsed with 1M NaCl solution, PBS, MQ water, ethanol, methanol, and dried in N_2 flow. This ensures that the CTAB is largely rinsed off the surface of the particles.

The functionalization of nanoparticles with ssDNA was performed using low-pH protocol on glass coverslip immediately after spincoating the particles. We used citric acid buffer of 10 mM strength, pH of 3, and 1 M of ionic strength, these conditions give very efficient functionalization performance. The total ssDNA concentration was kept at 5 µM, even in the case of the mixture of docking and antifouling strands, where the docking percentage was specifically tuned. We show the sequences in detail in Table S1. The ssDNA binds to gold nanoparticle via thiol – Au covalent bond. Therefore prior to the functionalization the thiolated-DNA was incubated in 1 mM of TCEP for 30 minutes to anneal possible di-thiol bridges. The incubation time was varied from few seconds to several days. Immediately after the incubation was finished the samples were extensively rinsed with PBS and MQ to get rid of residual ssDNA. Such sample was inserted into the flow cell right away and kept wet for the entire course of measurement. We performed all our experiments in the so-called Buffer C, which is PBS buffer with elevated ionic strength to 637 mM and pH of 7.2.

ssDNA strand	**Length**	**Sequence (from 5' to 3')**
Docking strand	30 nt	SH - CAT CAT CAT ACG CTT CCA AT A ATA CAT CTA
Antifouling strand	10 nt	SH - ACG CTA TCA G
Non-complementary strand	30 nt	SH - AAG ATG CTT ACG CTA CGA TTA CGC TAT CAG
Imager strand	10 nt (9 bp)	ATTO 647N – C TAG ATG TAT

Table S1: DNA sequences used in our experiments. Note that the imager strand is 10 nt long, however only 9 nucleotides contribute to the hybridization with the docking strand.

S2 Gold nanorods

We used commercially available colloidal nanorods from *Nanoseedz* stabilized with CTAB. They exhibit an ensemble-average longitudinal plasmon at 760 nm. Our single-particle measurements using hyperspectral microscopy (Figure S1a) then uncovers the entire distribution of individual plasmon wavelengths 765 +- 39 nm. For the detailed description of hyperspectral microscopy method we refer to our previous publication,[1] namely Supplementary information section S3. We characterized the geometrical properties of our nanorods by transmission electron microscopy (TEM). We probe a representative ensemble of 174 particles and found a distribution of diameter of 22 ± 4 nm and length of 75 ± 13 nm giving dispersions of ± 12.2 % and ± 17.3 %, respectively. This gives the underlying distributions of aspect ratio in our sample is 3.6 ± 1.0. As discussed later on, an important parameter for particle functionalization with biomolecules is the surface area of nanorods. We treated nanorods as spherically-capped cylinders and find the average surface area of 5100 +- 1400 nm^2 (see inset of Figure S1c).

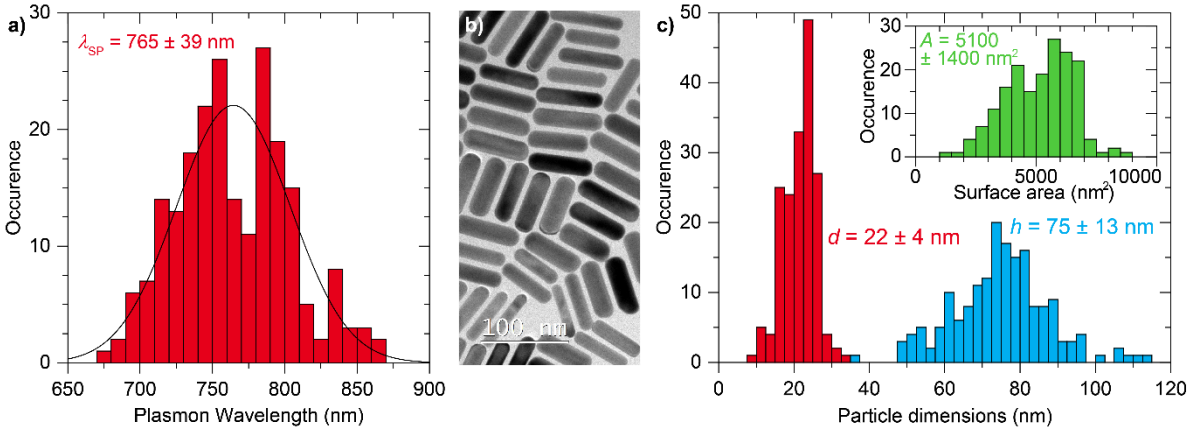

Figure S1: Used gold nanorods: **(a)** Histogram of longitudinal plasmonic wavelengths of individual single gold nanorods after ssDNA functionalization measured using hyperspectral microscopy. **(b)** TEM measurement of dried gold nanorods, the scale bar is 100 nm. **(c)** Histograms of nanorods' dimensions extracted from TEM measurements.

S3 Estimation of maximum loading of nanoparticles

To be able to understand the process of gold nanoparticle functionalization with ssDNA we develop an estimate of the maximal molecular loading of employed particles. We based ourselves on the work by Hill et al.[2] and consider thiolated DNA molecules as closely-packed cones occupying the space around a particle. A simplified sketch of the system geometry is depicted in Figure S2a with all important variables specifically marked. Based on TEM measurements we assume our nanorods to be spherically capped cylinders neglecting any surface irregularities. Since the particle functionalization with ssDNA is performed at high ionic strength (I = 1 M) where ssDNA adopts "mushroom-like" conformation, we approximate ssDNA by a sphere with its hydrodynamic radius $R_{\mathrm{H}} = R_{\mathrm{DNA}}$.

To get the maximal amount of molecular spheres which could fit around a nanorod we calculate the surface area of a layer distant R_{DNA} from the nanorod surface and divide this by the molecular footprint on the layer ($A_{\mathrm{DNA}} \approx \pi R_{\mathrm{DNA}}^2$). For the case of particles immobilized on a substrate their significant part of surface area is shielded from molecular binding. We correct for this effect by finding the minimal angle α:

$$\alpha = \cos^{-1}\left(\frac{d - 2R_{\mathrm{DNA}}}{d + 2R_{\mathrm{DNA}}}\right) - \frac{\varphi}{2} \quad , \quad \varphi = 2\sin^{-1}\left(\frac{2R_{\mathrm{DNA}}}{d + 2R_{\mathrm{DNA}}}\right) \quad , \tag{S1}$$

marking the inaccessible space, and discard the corresponding particle's surface area. The geometrical derivations lead to a following expression for maximal number of molecules on the surface a nanorod:

$$N_{max} = \frac{(d + 2R_{\mathrm{DNA}})^2}{R_{\mathrm{DNA}}^2}\frac{(1 + \cos\alpha)}{2} + \frac{(d + 2R_{\mathrm{DNA}})(h - d)}{R_{\mathrm{DNA}}^2}\frac{(\pi - \alpha)}{\pi} \quad . \tag{S2}$$

The Equation S2 clearly shows that particle loading is dependent on two parameters: the particle dimensions and the size of employed molecule. We obtained diameters and height of our nanorod using TEM in previous section. However a reliable estimate of molecular size for employed ssDNA is required. Single stranded DNA consist of individual nucleotides connected together through a phosphate backbone via flexible covalent bonds. This makes ssDNA an ideal candidate to be modeled using worm-like chain model.[3] In this model a polymer is considered to consist of n solid segments of which movement is allowed due to flexible linkers. In such case the measure of polymer length is the contour lenght $L_n = nl_{\mathrm{b}}$ which is the distance between the chain ends measured along the helical axis for each segment of length l_{b} ($l_{\mathrm{b}} = 0.63$ nm for ssDNA[4]). However the practical insight into the molecular size is given by the end-to-end length R_n which is the vector sum of each segment length[3]

$$\langle R_n^2 \rangle = 2P\left(L_n - P + Pe^{-\frac{L_n}{P}}\right) \quad , \tag{S3}$$

where P is the persistence length of the molecule. Since we deal with charged polymer we correct the persistence length for electrostatic charges[5]

$$P \cong P_0 + P_{\mathrm{OSF}} = P_0 + \frac{\lambda_{\mathrm{B}} f}{4\kappa^2} \quad , \tag{S4}$$

where P_0 is the bare persistence length (for ssDNA $P_0 \approx 2$ nm[4]), and $\lambda_{\mathrm{B}} = e^2/4\pi\varepsilon_{\mathrm{r}}\varepsilon_0 k_{\mathrm{B}}T$ is the Bjerrum length at which the electrostatic interaction between two point charges e is equal to the thermal energy $k_{\mathrm{B}}T$, and $f = z/l_{\mathrm{b}}$ is the fractional number of charges per segment length. Here, for the case of ssDNA $z = 1$ corresponding to one charge per nucleotide. The Debye length κ is the length at which salt ions screen the electric field, and for a monovalent electrolyte as i.e. NaCl is defined as:[6]

$$\frac{1}{\kappa} = \sqrt{\frac{\varepsilon_{\mathrm{r}}\varepsilon_0 k_{\mathrm{B}}T}{2N_{\mathrm{A}}e^2 I}} \quad . \tag{S5}$$

Here, ε_0 is the permittivity of vacuum, ε_{r} is the relative permittivity of the liquid (for water $\varepsilon_{\mathrm{r}} = 78.3$), k_{B} is the Boltzmann constant, T the temperature (here we consider $T = 298$ K), N_{A} the Avogadro constant and I is the ionic strength of the liquid.

The model shows that for low ionic strength the electrostatic interaction play significant role and extend the molecules in a stretched form characterized by long end-to-end distance. However, for the case of high ionic strength (I > 100 mM) the ions in the solution effectively shield the electrostatic repulsions between individual polymer segments reducing the end-to-end distance giving molecule a "mushroom-like" conformation. We approximate this complex shape by a hard sphere characterized by its hydrodynamic radius $R_{\mathrm{H}} = R_{\mathrm{DNA}}$ since this allows us to include electrostatic[5] and hydrodynamic[7] interactions. The diffusion coefficient D of such sphere is defined by Stokes-Einstein equation:[8]

$$D = \frac{k_{\mathrm{B}}T}{6\pi\eta_0 R_{\mathrm{DNA}}} \quad , \tag{S6}$$

and the diffusion coefficient of flexible polymers in dilute solutions is then given by the Zimm model:[7]

$$D = \frac{8k_{\mathrm{B}}T}{3\sqrt{6\pi^3}\eta_0 R_n} \quad , \tag{S7}$$

where η_0 is the viscosity of water $\eta_0 = 8.9 \cdot 10^{-4}$ Pa · s at $T = 298$ K). The Equation S6 and Equation S7 result in the expression for the molecular radius:

$$R_{\mathrm{DNA}} = \frac{3\sqrt{\pi}}{8\sqrt{6}} R_n \cong 0.271 R_n \quad . \tag{S 8}$$

We directly recalculate the molecular radius to ssDNA footprint for 30 nt long molecule and 1 M of buffer ionic strength and obtain $A_{\mathrm{DNA}} \approx 16$ nm^2 matching well the literature.[2] We further test our model against experimental results for ensemble measurements of ssDNA binding to gold spheres published by Hill et al.[2] and find an excellent match (Figure S2b). Note, that here we did not assume shielding by a present substrate. Having the confidence about reliability of our model we determine the maximal molecular loading for all nanorods measured with TEM. In Figure S2c we obtain a „normal-like" distribution of number of molecules over individual particles of $N_{\mathrm{max}} = 338 \pm 85$ characterized by a relative spread of 25 % owing to the size distribution of the sample that leads to a distribution of surface areas available for binding.

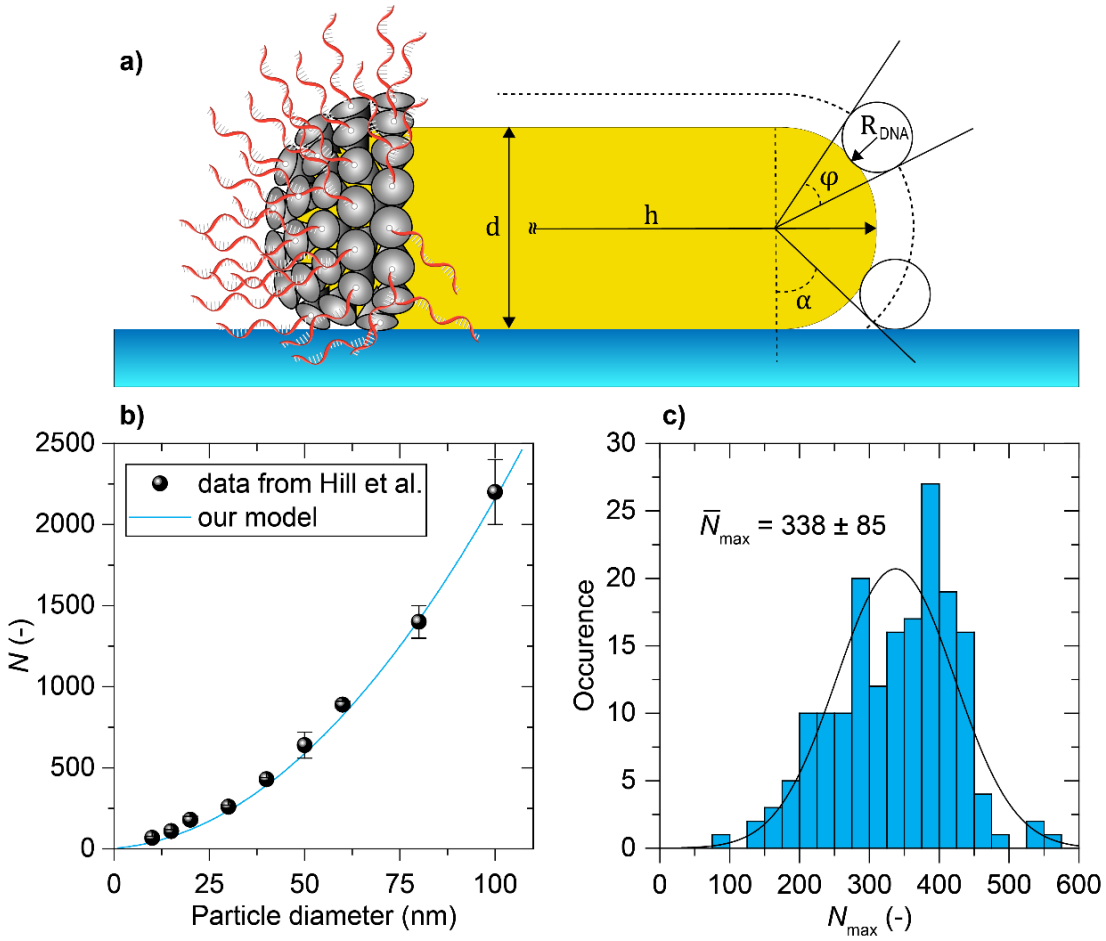

Figure S2: (a) Illustration of conical representation of thiolated ssDNA bounded to a nanoparticle with specified geometry of the system. **(b)** Testing our model against experimental data for ssDNA functionalization of gold spheres measured by Hill et al.[2] In this case we do not assume the presence of a substrate. (c) Histogram of maximal number of ssDNA molecules on individual gold nanorods for dimensions measured by TEM.

S4 Fluorescence excitation and spectra

The fluorophores transiently re-binding to/from gold nanorods are excited using a Coherent OBIS FP 637LX laser, which produces a laser light with a wavelength of 637 nm. Using a laser power of 110 mW, this results in a maximum laser power density of 1910 W/cm^2, assuming a Gaussian profile of the beam. As the fluorescent label we use the ATTO647N,[9] of which spectra can be seen in Figure S3.

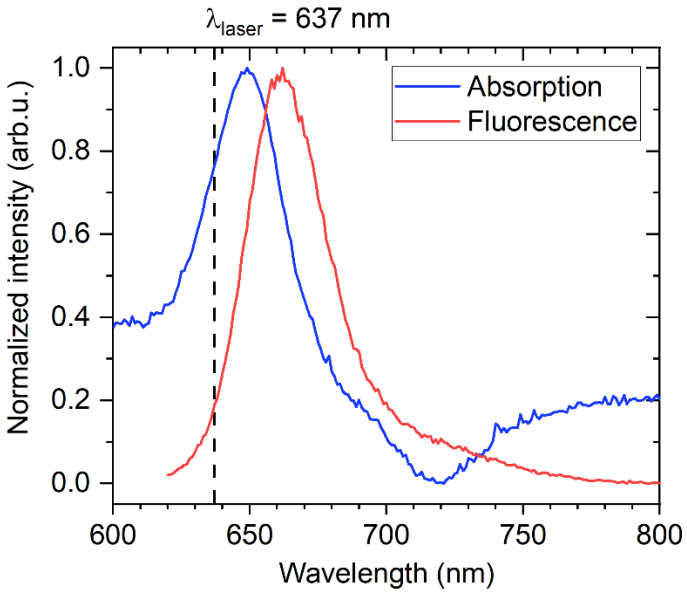

Figure S3: The absorption and emission spectra of the used fluorophore ATTO647N.[9] The dashed vertical line marks the wavelength of the excitation laser.

S5 Data processing - Event correction and localization

To identify individual events we first threshold the timetraces at $\mu + 4\sigma$, where intensity above this level is considered as an event. Due to high signal-to-noise ratio this step results in clearly distingushible signal distributions. Binding events can persist for multiple frames and therefore their start and end should be determined in detail.

We correct for a blinking and a re-binding of the individual imager causing undershooting of the average darktime (see second event in Figure S4a). This situation is considered to happen when signal fluctuates around the threshold level and stays at the baseline level just for a single time frame. Another correction is applied to fix a drop of the fluorescence signal below the threshold but not back to the baseline level (see third event in Figure S4a). In this case ten preceding and consecutive frames are being check if they exceed $\mu + 2\sigma$. We speculate that this feature possibly comes either from different time-averaged orientations of the dye with respect to incoming laser polarization at different time-frames, or from photobleaching of the dye. After correcting such events they are thus considered as one single molecular event.

Since our current analysis determines the fluorescence intensity by summing all pixels in small ROI around the nanoparticle (9x9 pxs), we do not yet resolve specific from nonspecific events which happen very close to (but not on) the nanoparticle. Therefore we super-localize the individual (already determined) fluorescent events by fitting them to 2D Gaussian. After gathering positions of all events per nanoparticle the corresponding location of the nanoparticle is determined. Per event, all ROI frames that persist above the threshold are merged together. This gives a summation of signal from both the bound fluorophore, and from the underlying nanorod's one-photon luminescence (1PL). This contribution from 1PL must be subtracted to yield the signal from only the fluorophore. The 1PL background is determined for every event individually by averaging the same amount of frames as the event but only containing the 1PL signal directly preceding the fluorescent event. By taking the 1PL background this way we minimize the effect of thermal drift. This process is depicted in Figure S4b, with a binding event detected above threshold, lasting for 17 frames and shaded in green. The Maximum Likelihood Method (MLE) is then used to fit a Gaussian[10] to the resulting point-spread-function, and extract the binding centroid.

After detection and super-localization of all events we corrected for a thermal drift. Drift correction was determined using set (~10) of fiducials, which are particles with very bright 1PL signal at 637 nm excitation, preferentially clusters. Their localizations is determined for each individual timeframe of the measurement by fitting to 2D Gaussian. The fiducials position timetraces are leveled-up, smoothened, and averaged out yielding a single position timetrace serving as the drift correction. For every single event the drift correction is determined individually by taking the average fiducial positions over the event bright time, and subtracted from the position of the event. This gives true location of the fluorophore.

Further we apply spatial density filter on the drift-corrected localizations and discard every event isolated within radius of 50 nm. Followed by accumulating all remaining localizations we reconstruct the particle localization cloud by fitting an error ellipse[11] to the localizations. Three different examples of typical particle clouds are shown in Figure S4c. The error ellipse fit estimates diameter, height, and orientation of the nanorod. We further approximate the ellipse lineshape by a 2D projection of spherically capped cylinder and determine all events happening inside this shape. These events are finally proceeded to determine dark times distribution and the number of binding sites on the nanoparticle.

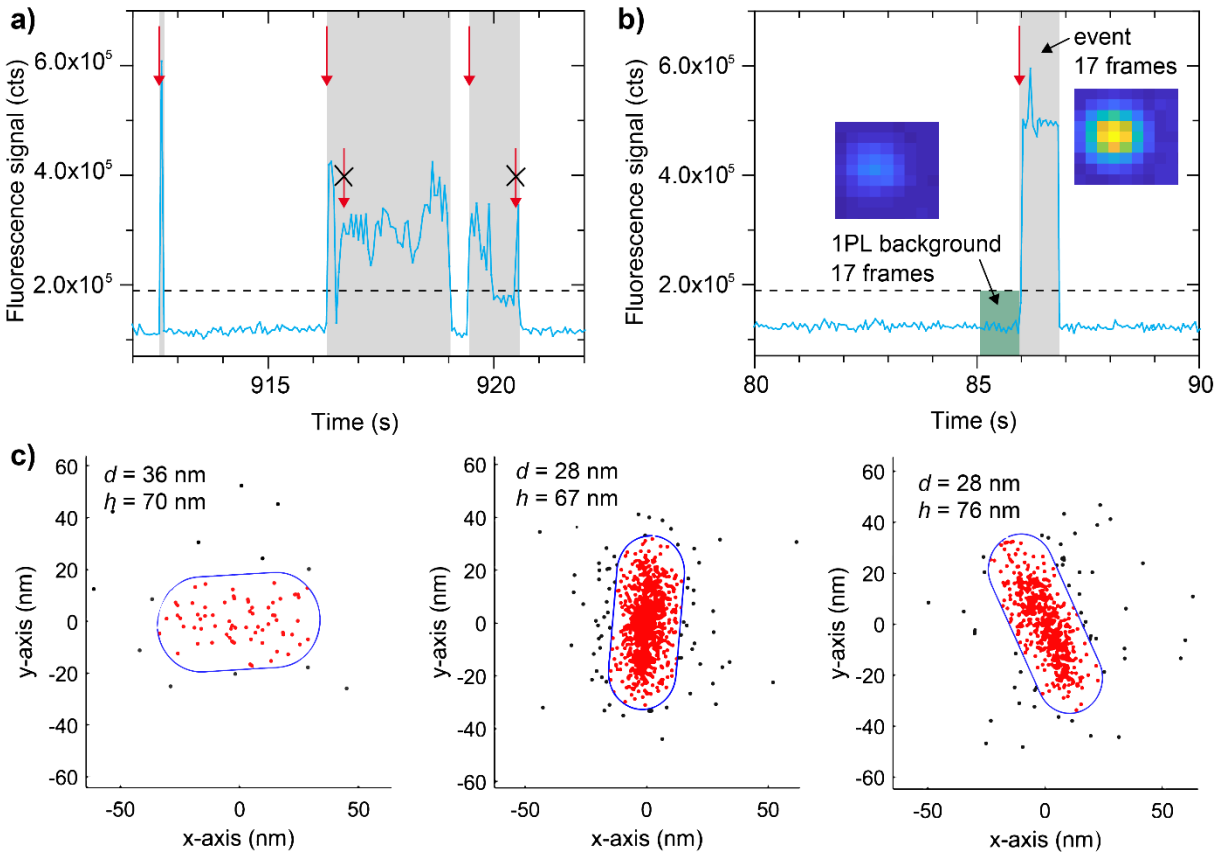

Figure S4: (a) Detection of fluorescent events and subsequent correction of rebinding and signal fluctuation. **(b)** Scheme of 1PL background subtraction. Shown 9x9 px ROIs show 17 merged frames of 1PL background (left) directly preceeding the fluorescent event (right). **(c)** Three examples of particle localization clouds with corresponding error-ellipse fit determining particles' diameters and heights.

S6 Control experiments and reproducibility

We address the specificity of single molecular interactions in our system. A typical experimental timetrace of fluorescently labeled imager strands stochastically binding and unbinding to docking strands on a single gold nanorod is shown in Figure S5a (cyan). The identified and corrected fluorescence bursts are subsequently super-localized and the particle localization cloud is determined. *Figure 2e* from the main text illustrates that imager strands bind dominantly to the functionalized nanorods with minimal non-specific binding to the glass coverslip. We take single-molecular events happening inside the localization cloud and extract their bright times to determine if the fluorescence signal is due to specific DNA hybridization. In Figure S5b we find mean bright time of $\tau_b = 550 \pm 275$ ms corresponding to the mean dissociation rate of $k_{\text{off}} = 2.2 \pm 1.0$ s^{-1} well matching the literature.[12]

To further ensure that the fluorescent events we observe are due to specific DNA hybridization between the docking and the imager strands we performed control experiments on nanoparticles functionalized with ssDNA strand with a sequence non-complementary to the imager strand. We functionalized gold nanorods with thiolated 30 nt non-complementary strand and 10 nt antifouling strand from 5 μM for 1 hour in citric acid buffer. Subsequently we measured their fluorescence signal with 1 nM of imager strand in solution. Control measurements did not show any consistent stochastic imager hybridizing, only very few molecular events were detected corresponding mostly to binding outside the particle's localization cloud as shown on examples in Figure S5a. We extracted darktimes between the residual events inside the particle cloud and reconstructed histograms of number of residual binding sites (Figure S5b,c). We report relatively narrow distributions characterized by a low mean of 0.4 and 0.8 binding sites, respectively, with majority particles showing no detected fluorescence events thus zero binding sites. However the determined number of non-specific binding sites suffer from high statistical error since only few events were recorded on individual nanoparticles over 90 minutes of measurement. These observations conclude that we resolve individual single molecular DNA hybridization events and contribution of the non-specific events is negligible.

Now we focus on reproducibility of our measurements. We prepared three distinct samples of nanoparticles functionalized with thiolated docking stands at 5 μM for one hour in citric acid buffer of pH 3. The samples were prepared at same chemical conditions, however at different days. Subsequently we measured the number of binding sites on individual nanorods and extracted dark times between single-molecular events. Histograms of binding site numbers for different samples are plotted in Figure S6. We note, that here we do not apply the localization filter. In all three cases we find normal-like distributions characterized by similar means and spreads. These findings show very high reproducibility of our method and measurements, where all three obtained distributions show their means within the standard deviations. Samples 1 and 2 show similar coefficient of variation of ~ 29 %, however the Sample 3 is characterized by increased heterogeneity of 38 % which we relate to the lack of statistic for this sample.

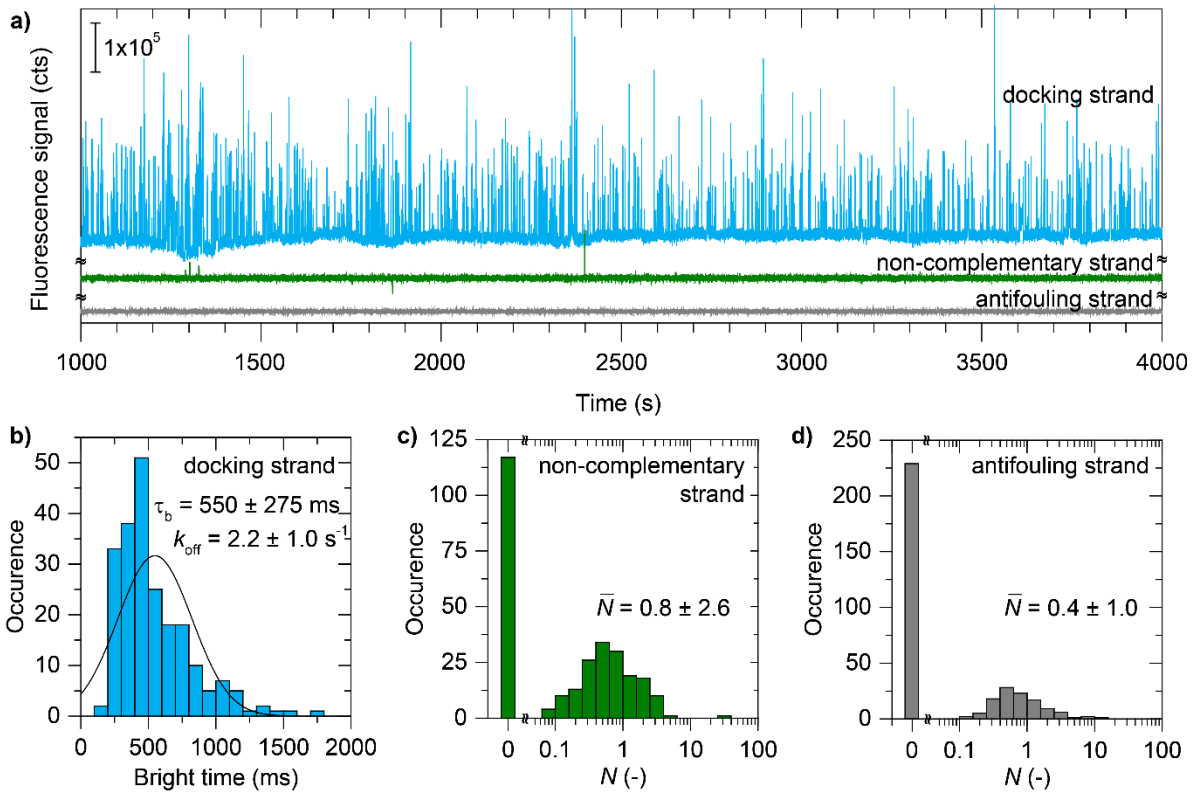

Figure S5: (a) Examples of typical timetraces for particles functionalized with specific docking strand (cyan), and non-complementary 30 nt and antifouling strands. **(b)** Histogram of particle mean bright times determines the k_{off} of DNA hybridization. Histograms of number of binding sites are determined from 90 minutes measurement at 1 nM of imager for particles functionalized with 30 nt non-complementary strands **(c)** and 10 nt antifouling strands **(d)**.

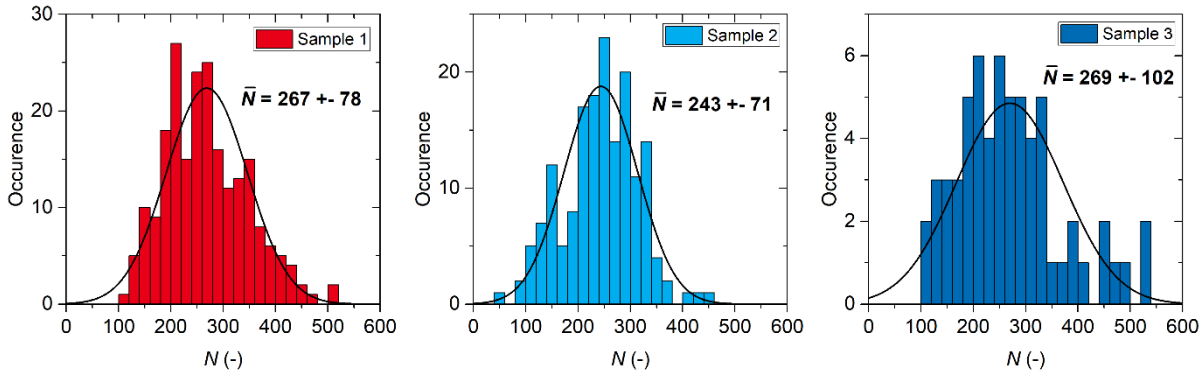

Figure S6: Reproducibility of measurements. Three different samples of gold nanorods functionalized with ssDNA docking strands at 5 µM using low pH coupling method.

S7 Salt-aging coupling protocol

Optimization of functionalization protocols of thiolated DNA to gold nanoparticles has received considerable attention with the aim to understand and optimize the coating density. Dense coatings of thiolated ssDNA on gold nanoparticles were conventionally achieved using the so-called salt-aging method,[2,13,14] in which the electrostatic repulsion due to the negative charges on the gold particles and the ssDNA is gradually reduced by stepwise addition of salt over 1 or 2 days. Later it was shown that this process can be accelerated by orders of magnitude by reducing the pH of the employed buffer.[15,16] We used this so-called „low pH“ method in our study, here, we compare our results to the salt-aging method.

We used phosphate buffer of 20 mM strength, pH of 8, where the total docking strand concentration at the end of the coupling is 5 μM. Prior to the functionalization the thiolated ssDNA was incubated in 1 mM of TCEP for 30 minutes to anneal possible di-thiol bridges. The mixture was pipetted on glass immobilize gold nanorods, and then allowed to equilibrate for 20 min before bringing the NaCl concentration to 1 M over an 6 h period in a stepwise manner. After that the solution was left on nanorods overnight to allow further binding of docking strands. Immediately after the incubation was finished the samples were extensively rinsed with PBS and MQ to get rid of residual ssDNA. Such sample was inserted into the flow cell right away and kept wet for the entire course of measurement. We performed our experiments in PBS buffer with elevated ionic strength to 637 mM.

We measured the number of binding sites on individual nanorods and extracted dark times between single-molecular events. Histograms of binding site numbers is plotted in Figure S7. We note, that here we did not apply the localization filter during the analysis. We find mean number of binding sites of $\bar{N} = 281 \pm 126$ per individual nanoparticle giving relative spread of 45 %. Our low pH docking strand coupling was also performed at 1 M of ionic strength. This allows us to directly compare the results obtained for the salt-aging method in Figure S7 with the results for the low pH coupling method we investigated in detail in Figure S6. We report similar mean docking density within standard deviations. However the heterogeneity of the salt-aging functionalization increased in average by a factor 2 comparing to the low pH coupling.

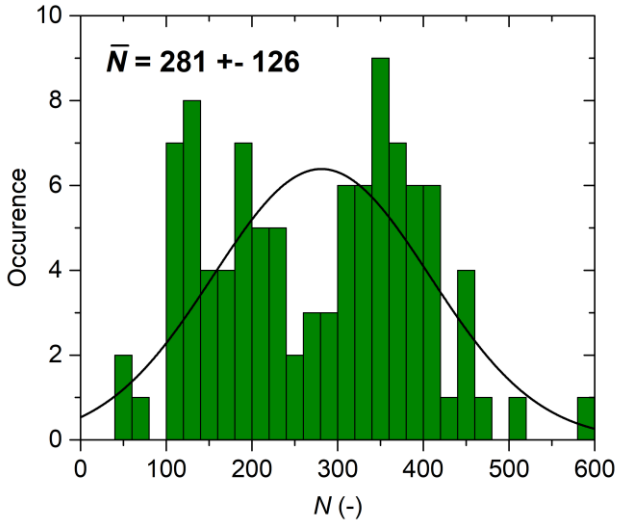

Figure S7: Number of binding sites per individual nanorods for salt-aging coupling protocol.

S8 Ligand reorganization – 100 % docking functionalization

In the main text we observe a substantially greater reduction of observed binding sites over long incubation times than predicted by literature[17] for particles functionalized with 1 % docking solution (*Figure 6a* in the main text). We further examine nanoparticles functionalized with only docking strand. We incubated our gold nanorods with thiolated docking strands at low pH for one hour, subsequently washed the residual unbound DNA and left the functionalized particles in pure citric acid buffer for two days. In Figure S8 the obtained results (green distribution) are directly compared to the results for 1 hour (pink) and two continuous days (cyan) of docking strand incubation. Comparing one hour (pink) and 2 days (cyan) incubation conditions we report a moderate decrease in the mean number of binding sites. Nevertheless, the important results we report for the functionalization conditions of one hour incubation and two subsequent days in the pure buffer. We see comparable functionalization heterogeneity with the two previous conditions, but the mean number of binding sites of the green distribution decreases by ~ 50 % comparing to the pink and cyan ones. These results rule out the thiol release as the main mechanism to the gradual reduction in the number of counted docking strands.

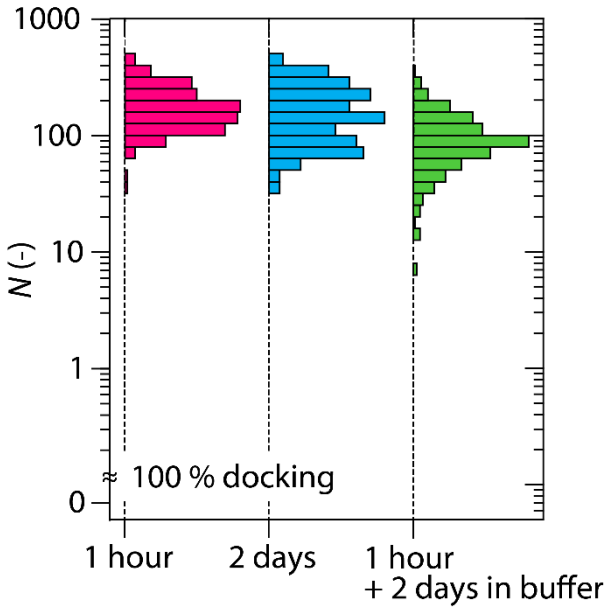

Figure S8: Ligand reorganization evidenced by the incubation of samples in DNA solutions with 100% docking strand for 2 days, and in DNA solution for 1 hour followed by incubation in buffer for 2 days.

S9 References

1 M. Horáček, R. E. Armstrong and P. Zijlstra, *Langmuir*, 2018, **34**, 131–138.
2 H. D. Hill, J. E. Millstone, M. J. Banholzer and C. a. Mirkin, *ACS Nano*, 2009, **3**, 418–424.
3 S. F. E. M. Doi, *The theory of Polymer Dynamics*, Clarendon Press, Oxford, 1998th edn., 1998.
4 E. W. A. Visser, *Biosensing Based on Tethered Particle Motion*, Eindhoven University of Technology, Eindhoven, 2017.
5 R. R. Netz and D. Andelman, *Phys. Rep.*, 2003, **380**, 1–95.
6 W. R. S. W. B. Russel, D. A. Saville, *Colloidal Dispersions*, Cambridge University Press, Cambridge, 1989.
7 B. H. Zimm, *J. Chem. Phys.*, 1956, **24**, 269–278.
8 J. N. Israelachvili, *Intermolecular and Surface Forces*, Elsevier, Amsterdam, 3rd editio., 2011.
9 ATTO-TEC GmbH, https://www.atto-tec.com/, https://www.atto-tec.com/product_info.php?info=p114_atto-647n.html, (accessed 20 January 2020).
10 K. I. Mortensen, L. S. Churchman, J. A. Spudich and H. Flyvbjerg, *Nat. Methods*, 2010, **7**, 377–381.
11 W. K. R. K. Bock, *The Data Analysis Briefbook*, Springer, Berlin, 1998.
12 R. Jungmann, C. Steinhauer, M. Scheible, A. Kuzyk, P. Tinnefeld and F. C. Simmel, *Nano Lett.*, 2010, **10**, 4756–4761.
13 S. J. Hurst, A. K. R. Lytton-Jean and C. a Mirkin, *Anal. Chem.*, 2006, **78**, 8313–8.
14 L. M. Demers, C. A. Mirkin, R. C. Mucic, R. A. Reynolds, R. L. Letsinger, R. Elghanian and G. Viswanadham, *Anal. Chem.*, 2000, **72**, 5535–5541.
15 X. Zhang, M. R. Servos and J. Liu, *J. Am. Chem. Soc.*, 2012, **134**, 7266–7269.
16 X. Zhang, T. Gouriye, K. Göeken, M. R. Servos, R. Gill and J. Liu, *J. Phys. Chem. C*, 2013, **117**, 15677–15684.
17 F. Li, H. Zhang, B. Dever, X. F. Li and X. C. Le, *Bioconjug. Chem.*, 2013, **24**, 1790–1797.